

Image Enhancement with Polymer Grid Triode Arrays

Alan J. Heeger, David J. Heeger,* John Langan, Yang Yang

An array of polymer grid triodes connected by a common grid functions as a "plastic retina," providing local contrast gain control for image enhancement. This simple device, made from layers of conducting polymers, functions as an active resistive network that performs center-surround filtering. The polymer grid triode array with common grid is a continuous analog of the discrete approach of Mead, with a variety of fabrication advantages and significant savings in area within the unit cell of each pixel.

When a person views a brightly lighted external scene through a window from inside a poorly lighted room, the individual has no difficulty seeing simultaneously the details of both the internal scene and the external scene. This is done by local contrast control; the visual system locally adjusts the gain using lateral inhibition.

Consider the office scene in Fig. 1. When the original (14-bit) image is displayed with only the dynamic range available on the printed page (about 8 bits) (Fig. 1A), gray regions greater than 255 are clipped (set to 255), simulating saturation in the region of highest brightness. When the image is rescaled (the intensity of each pixel was divided by 8) and displayed over the same dynamic range (Fig. 1B), it is analogous to the image shown on a video display with reduced gain; the features are visible only in the background (bright) regions. In both cases, a great deal of information contained in the original (14-bit) image is lost: in Fig. 1A, the viewer cannot see any detail in the bright regions of the image, and in Fig. 1B, the viewer cannot see any detail in the darker regions of the image.

Local contrast control involves a combination of logarithmic compression and lateral inhibition, the latter provided by a horizontal resistive network (a neural network) (1, 2). After logarithmic compression, the output (V_i) from a given pixel i is proportional to the log of the intensity (I_i) of that pixel

$$V_i = V_0 \log I_i \quad (1)$$

where V_0 is the constant of proportionality. Lateral inhibition is implemented by subtracting from V_i the average of the surrounding values; thus, the renormalized image is defined by

$$\begin{aligned} v_i &= V_0 \log I_i - \langle V_0 \log I_i \rangle \\ &= V_0 \log I_i - \frac{V_0}{N} \sum_i \log I_i \end{aligned} \quad (2)$$

where the brackets denote an average value and the sum is over neighboring pixels within the averaging range (the center-surround or blurring range). Equation 2 is equivalent to

$$v_i = V_0 \log \left[\frac{I_i}{(\prod I_i)^{1/N}} \right] \quad (3)$$

The denominator is the geometric mean. Equation 3 is the mathematical expression of Mead's local contrast enhancement algorithm (1); it can be generalized to allow for a weighted average by replacing $1/N$ by w_i , where w_i are the weights.

If the original image of the office scene is processed with the Mead algorithm (Fig. 1C), one can see details in the entire image even within the limited range available on the printed page. The simulations in Fig. 1 demonstrate the power of local contrast enhancement.

In this report, we show that the local contrast enhancement algorithm (Eqs. 2 and 3) can be implemented with a simple device made from layers of conducting polymers. The device consists of an array of polymer grid triodes (PGTs) (3) connected through a common grid, which serves as a resistive network.

In a layered thin-film PGT (Fig. 2A), the top layer (5) is the anode and the bottom layer (1) is the cathode. The third electrode (3), analogous to the grid in a vacuum tube triode, is an open network of polyaniline (PANI) protonated to the highly conducting form with camphor sulfonic acid (CSA) (3). Semiconducting polymer forms layers 2 and 4, between the anode and the polymer grid and between the polymer grid and the cathode, and fills the void spaces within the porous PANI-CSA network (3').

An array of PGTs with a common grid (Fig. 2B) can perform local contrast enhancement like that simulated in Fig. 1. Because the thin films that constitute the PGT array can be processed from solution, they can be layered directly on an array of photodetectors. Each node of the PGT array corresponds to one pixel of the image. The array of PGTs with a common grid performs three important functions: (i) The

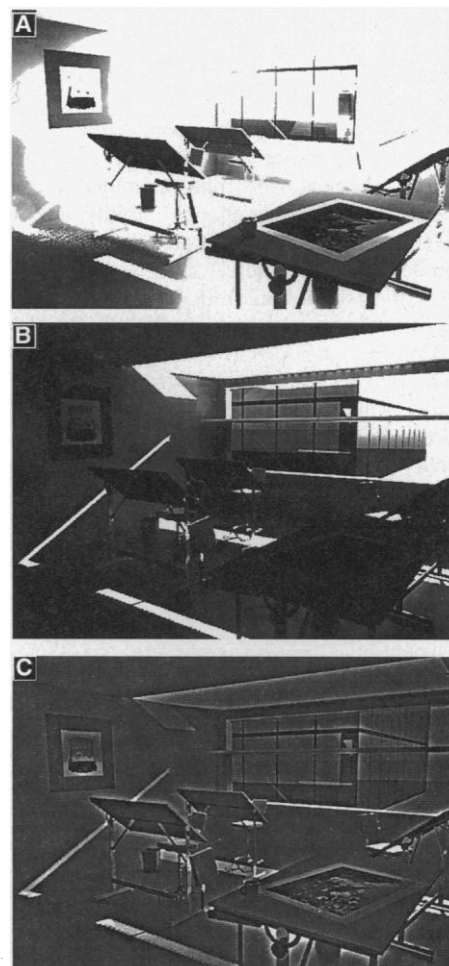


Fig. 1. (A) Original (14-bit) image of an office scene displayed with only the dynamic range available on the printed page (about 8 bits). Gray values greater than 255 were clipped (set to 255). Features are visible only in the foreground (dark) regions. (B) The same image, rescaled (the intensity of each pixel was divided by 8) and again displayed with the dynamic range available on the printed page (again, gray values greater than 255 were clipped). Features are clearly visible only in the (bright) background. (C) The result of using local contrast gain control on the office scene. The 14-bit image was renormalized with Eq. 3 and a Gaussian-weighted average over a 13 pixel by 13 pixel neighborhood. Features are now visible throughout the image.

common grid functions as a resistive network that computes the blurring (averaging) in Eq. 2. (ii) The output current at one node of the PGT array is approximately the difference between the input anode-to-cathode voltage and the local grid voltage. Because the local grid voltage is the local average [see (i)], the PGT array acts as a center-surround filter (1, 2) that computes the difference in Eq. 2. (iii) The PGT array with common grid provides the high input resistance needed for open circuit detector operation (4), which results in the logarithmic compression in Eq. 2.

UNIAx Corporation, 6780 Cortona Road, Santa Barbara, CA 93117, USA.

*Permanent address: Department of Psychology, Stanford University, Stanford, CA 94305, USA.

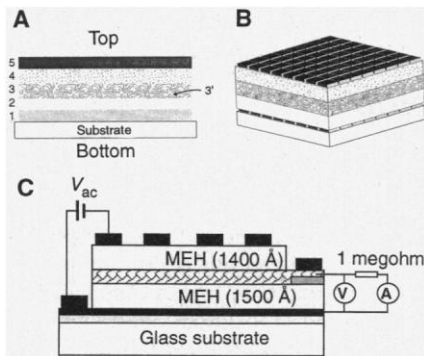


Fig. 2. (A) Structure of the PGT. Layers **1** and **5** are the cathode and anode (pixel) arrays, respectively. The other layers are continuous films common to all the PGTs within the array: **2** and **4** are semiconducting layers, poly(2-methoxy-5-(2'-ethyl-hexyloxy)-1,4-phenylene vinylene) (MEH-PPV), and **3** is the common grid network filled with semiconductor (**3'**). (B) Schematic diagram of an array of PGTs with a common grid. Thickness (between anode and cathode) is about $0.3 \mu\text{m}$. Each anode-cathode pad is, for example, $50 \mu\text{m}$ on a side. (C) Four PGTs in an array with a common grid.

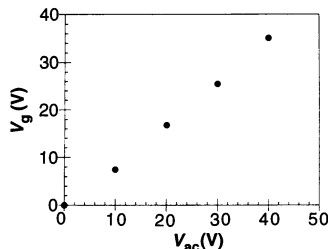


Fig. 3. Grid voltage V_g is proportional to input voltage applied at neighboring positions, that is, the grid voltage provides a local average; the voltage V_{ac} is applied between the anode and cathode on the left of the array, and V_g is measured near the rightmost triode of the array (Fig. 2C).

Thus, local contrast enhancement, as described by Eqs. 2 and 3, can be directly implemented with the PGT array in Fig. 2B. The effective computation rates involved are impressive: The equivalent calculation implemented on a serial computer would require about 40 million multiplications per second (256×256 pixels, 30 frames per second, 13×13 blurring with separable convolution).

We have fabricated PGT arrays with four triodes on a single substrate, all with a common grid (Fig. 2C). The fabrication process for the triode array is similar to that of a single PGT (3); the principal difference is that there are separate contact pads for each device in the array. For the arrays fabricated in this study, the sheet resistance of the common grid was about 20 kilohms per square.

The voltage of the common grid (V_g) with respect to the anode was measured

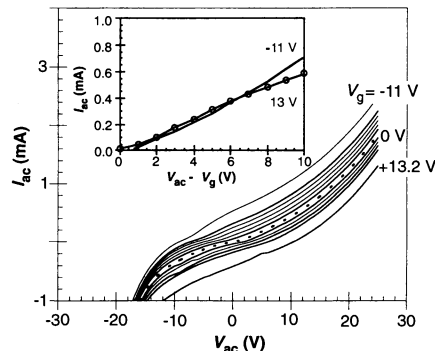


Fig. 4. The I_{ac} versus V_{ac} curves for different grid voltages (V_g). (Inset) The two limiting data sets [$V_g = -11 \text{ V}$ (solid line) and $V_g = +13.2 \text{ V}$ (line with circles)] as a function of $V_{ac} - V_g$.

while a voltage (V_{ac}) was applied between the anode and the cathode of the left triode (Fig. 2C). The voltage of the common grid was measured near the neighboring triode on the far right; V_g at this neighboring position responds in proportion to V_{ac} (Fig. 3) such that $V_g = \beta \langle V_{ac} \rangle$ (where β is a constant of proportionality), that is, the grid voltage responds to the local input and provides a local average.

The final step required to demonstrate the validity of the PGT implementation of local contrast enhancement is to show that it computes the center-surround difference in Eq. 2. The equivalent circuit of the PGT (3) is two coupled diodes connected back-to-back, like a bipolar transistor (4). This is achieved by using semiconducting polymer in layers 2, 3', and 4. For the prototype array sketched in Fig. 2C, layer 2 was fabricated with a material of sufficient conductivity to make an ohmic contact to the grid, so that the equivalent circuit is simplified to a diode in series with a resistor. In the initial experiments, polyvinylcarbazole (PVK) was used for resistor layer 2. In forward bias

$$I = I_0 e^{\gamma(V_{ac} - V_g)} + \frac{(V_{ac} - V_g)}{R_s} + \frac{V_g}{R_i} \quad (4)$$

where γ is a constant (3), R_i is the internal series resistance of the diode (from the bulk resistivity of the semiconducting material used in 4), and R_s is the series resistance resulting from the PVK layer (2). Because the semiconducting layer is fabricated from a high-resistivity, pure semiconducting polymer such as poly(phenylene vinylene) (PPV) or one of its soluble derivatives, $R_s \ll R_i$. Thus, the output of the PGT is a function of $V_{ac} - V_g$ only; that is,

$$I = F(V_{ac} - V_g) \quad (5)$$

This is demonstrated by I versus V_{ac} data for different V_g (Fig. 4). As expected, the curves are sensitive to V_g ; for example, at

$V_{ac} \approx 5 \text{ V}$, the current can be suppressed from 1 mA to zero by changing V_g . In the inset to Fig. 4, we replotted the curves from the two limiting data sets ($V_g = -11 \text{ V}$ and $V_g = +13.2 \text{ V}$) as a function of $V_{ac} - V_g$. Because the forward-bias data collapse onto a single curve, Eq. 5 is indeed valid. Consider then the array of PGTs, with common grid, sketched in Fig. 2B, and assume, for simplicity, that the common grid is grounded at infinity. Because of the common grid

$$V_g = \beta \langle V_{ac} \rangle \quad (6)$$

where $\langle V_{ac} \rangle$ denotes the average over neighboring pixels with a distance determined by the sheet resistance of the grid and the conductance to ground of the resistive layer (in this case, PVK). The characteristic length over which the average is taken (1) is given by

$$L = 1/(\rho\sigma)^{1/2} \quad (7)$$

where ρ is the sheet resistance of the PANI network grid and σ is the conductance per unit area to ground through the resistive PVK layer.

We conclude that the current output from each pixel of the array is given by

$$\begin{aligned} I_i &= F(V_{ac}^{(i)} - \beta \langle V_{ac} \rangle) \\ &\approx (V_{ac}^{(i)} - \beta \langle V_{ac} \rangle) (\partial F / \partial V) \end{aligned} \quad (8)$$

Equation 8 is equivalent to Eq. 3 provided that the output of each detector on the focal plane array $V_A^{(i)}$, which serves as input to an individual pixel i , is proportional to the logarithm of the intensity: $V_A^{(i)} \propto \log I_L^{(i)}$, where $I_L^{(i)}$ is the intensity of the light incident on the i th pixel. Because $V_{out} \propto \log I_L$ for photovoltaic detectors under open circuit conditions, the logarithmic compression of Eq. 1 is straightforward (4).

The PGT-array image processor differs fundamentally from those built with discrete silicon field-effect transistors (1, 2). The PGT array makes use of the spreading resistance of the PANI control-grid network to provide the interconnection of a given node to its neighbors; the conductivity of the PANI network enables center-surround filtering as a result of lateral charge redistribution initiated by contrast differences. Charge redistribution through a continuous layer of material provides a natural means for averaging (blurring).

By controlling the concentration of PANI in the network, one can control the resistivity over many orders of magnitude (5). Similarly, by varying the thickness and the resistivity of layer 2, by back biasing the grid-to-ground diode during operation or by making 2 a bilayer that functions as a diode with the use of conducting polymers (6), one can vary the conductance of layer 2 over a wide range. The latter is particularly

interesting because it allows in situ dynamic control of the spatial decay length. Thus, one can vary both ρ and σ (Eq. 7) so as to achieve values for L (either statically or dynamically) ranging from a few micrometers to 1 cm.

We have shown that this simple device, made from layers of conducting polymers, provides both logarithmic compression and lateral inhibition of response, as required for local contrast control. Nevertheless, the plastic retina is at an early stage of development. The utility of the PGT array for image enhancement will depend on a number of factors—including, for example, sensitivity, noise, dynamic range, and matching from one pixel to the next—that must be tested on an engineering prototype.

For a full plastic retina, the PGT image enhancement array would be fabricated directly onto the output side (back) of a photodetector array (for example, an infrared detector array) with each detector output pad as the anode or cathode of the PGT at that node. The semiconductor layers would be cast sequentially from solution and applied onto the detector array much like an antireflection coating. The final contrast-enhanced output would be connected to a demultiplexer by “bump bonding”; that is, by cold-welding indium bumps arrayed reciprocally on the PGT array output and on the demultiplexer input.

Alternatively, the PGT array could be used to process the image after analog-to-digital conversion and integrated directly into a display (such as a liquid-crystal display). In this case, the PGT array would be fabricated directly on, as an integral part of, the display: for example, between the control circuits and the liquid-crystal layer. The data would be logarithmically compressed digitally and input into the PGT array to process the image; the output from the pixels of the array of PGTs would serve as the input to the pixels of the display.

REFERENCES AND NOTES

1. C. Mead, *Analog VLSI and Neural Systems* (Addison-Wesley, Menlo Park, CA, 1989).
2. C. Koch and H. Li, Ed., *Vision Chips: Implementing Vision Algorithms with Analog VLSI Circuits* (IEEE Computer Society Press, Los Alamitos, CA, 1994).
3. Y. Yang and A. J. Heeger, U.S. patent application 08227,979; *Nature* **372**, 244 (1994).
4. S. M. Sze, *Physics of Semiconductor Devices* (Wiley, New York, 1981).
5. M. Reghu *et al.*, *Phys. Rev. B* **50**, 13931 (1994).
6. I. D. Parker, *J. Appl. Phys.* **75**, 1656 (1994); G. Yu, K. Pakbaz, A. J. Heeger, *Appl. Phys. Lett.* **64**, 3422 (1994), and references therein; H. Tomozawa, D. Braun, S. D. Phillips, A. J. Heeger, *Synth. Met.* **22**, 63 (1987).
7. The images in Fig. 1 were generated with the Radiance computer graphics rendering program, developed by G. Ward and funded by the Lighting Group at Lawrence Berkeley Laboratory, U.S. Department of Energy, and the Laboratory d'Energie Solaire et de Physique du Batiment at the Ecole Polytechnique Federale de Lausanne in Switzerland.

29 June 1995; accepted 3 October 1995

Laser-Driven Movement of Three-Dimensional Microstructures Generated by Laser Rapid Prototyping

Olaf Lehmann and Michael Stuke*

Three-dimensional microstructures consisting of aluminum oxide and aluminum were fabricated by laser-induced direct-write deposition from the gas phase. Trimethylamine alane and oxygen were used as precursors. Thermal expansion forces resulting from suitable laser irradiation were used to drive the movement of microstructure parts. Applications include micromechanical actuators, such as microtweezers and micromotors. The one-step nature of the laser direct-write process allows rapid prototyping of such devices.

Lithography and etching techniques that were originally developed for microelectronics applications can also be used to fabricate sensors, actuators, or other micromechanical devices on silicon. However, these techniques require photo masks to be made before the microstructures can be produced, and the production itself consists of many complicated and time-consuming steps—for example, because vertical structure variations can be performed only indirectly. Structural redevelopment often requires redesign of the masks. As a result, such techniques are economical mainly for mass production of devices that do not need any further development. Other mask-based techniques, such as the x-ray deep etching technique LIGA (Lithographie, Galvanoförmung, Abförmung), also suffer from this drawback.

As a result, methods for the single-step generation of three-dimensional (3D) microstructures have recently received considerable attention. The idea is to design a structure with the use of computer-aided technologies and to transfer the data directly to a machine, which then automatically generates a solid structure. This so-called rapid prototyping enables very fast evolution of structures, particularly when laser direct writing is used as a processing tool. Techniques based on photopolymerization or powder sintering have already been used in rapid prototyping of commercial products, but they offer only submillimeter resolution. Another possibility is fast layer-by-layer laser etching of silicon in chlorine, which can be performed with a resolution of 1 μm (1).

Laser-assisted chemical vapor deposition (LCVD) has been shown to be suitable for rapid prototyping with micrometer resolution (2). The method enables fabrication of thin rods and fibers by pulling the substrate

away from the stationary laser focus at a speed equal to the linear growth speed of the material, keeping the laser focus on the rod tip (3). LCVD was first demonstrated for carbon (4) and silicon (5) rods, but it has also been applied to the production of long carbon (6), silicon (7), and boron (8) fibers. More complex structures such as microsprings (9) have been obtained by moving the substrate on a bent track with the use of a goniometer, instead of simply pulling it linearly. Recently, we used two intersecting laser beams to create complex 3D microstructures consisting of aluminum oxide rods (10); our technique enables direct writing in free space in virtually any direction, as explained below.

When only one laser beam is used, LCVD can only create rods parallel or nearly parallel to the incident beam. To obtain rods in any direction, it was necessary to modify the technique. In weakly absorbing materials such as alumina, the absorption length of the laser light is large; the resulting uniform temperature distribution in the illuminated region leads to nondirectional material depo-

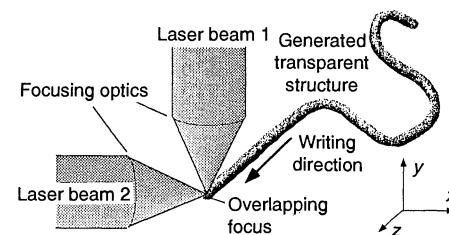


Fig. 1. Three-dimensional direct-write principle. The nearly transparent alumina rod absorbs the laser light only weakly, and thus most of the energy is absorbed in the bulk rather than at the surface. The laser beams are attenuated so that almost no growth is observable for either beam alone. The temperature rise causes nondirectional alumina deposition from the gas phase only in the area of overlapping focus, where the temperature threshold is exceeded. The writing direction is defined by slow ($\sim 10 \mu\text{m s}^{-1}$) movement of the laser focus.

Max-Planck-Institut für Biophysikalische Chemie, P.O. Box 2841, D-37018 Göttingen, Germany.

*To whom correspondence should be addressed.